Design and fabrication of adiabatic vertical couplers for hybrid integration by flip-chip bonding

Jinfeng Mu*[a], Mustafa A. Sefunc[a], Bojian Xu[b], Meindert Dijkstra[a], Sonia M. Garcia-Blanco[a]
[a]Optical Sciences Group, [b]Nanoelectronics Group, MESA+ Institute for Nanotechnology,
University of Twente, P.O. Box 217, 7500 AE Enschede, The Netherlands

ABSTRACT

Rare-earth ion doped crystalline potassium double tungstates, such as $KY(WO_4)_2$, $KLu(WO_4)_2$ and $KY(WO_4)_2$, exhibit many properties that make them promising candidates for the realization of lasers and amplifiers in integrated photonics. One of the key challenges for the hybrid integration of different photonic platforms remains the design and fabrication of low-loss and fabrication tolerant couplers for transferring light between different waveguides. In this paper, adiabatic vertical couplers realized by flip-chip bonding of polymer waveguides to Si_3N_4 devices are designed, fabricated and tested. An efficient design flow combining 2D and 3D simulations was proposed and its validity was demonstrated. The vertical couplers will ultimately be used for the integration of erbium doped $KY(WO_4)_2$ waveguides with passive platforms. The designed couplers exhibit less than 0.5 dB losses at adiabatic angles and below 1 dB loss for ±0.5 μm lateral misalignment. The fabricated vertical couplers show less than 1dB losses in average for different adiabatic angles of Si_3N_4 tapers, which is in good quantitative agreement with the simulations.

Keywords: hybrid integration, vertical coupler, mode overlap, flip-chip bonding, SU-8, silicon nitride

1. INTRODUCTION

Rare-earth ion doped monoclinic potassium double tungstates, such as $KY(WO_4)_2$, $KLu(WO_4)_2$ and $KY(WO_4)_2$, are recognized as excellent gain materials for the realization of lasers and amplifiers thanks to the large gain bandwidth and long excited state lifetime [1] of the rare-earth ions in combination with the high gain per unit length [2] achievable when the rare-earth ions are doped into these type of crystalline host materials. The relatively large optical bandwidth and energy storage capacity is favorable for mode-locking and short pulse generation [3]. A high output power of 1.6 W has been recently demonstrated in a highly efficient Tm^{3+} doped potassium double tungstate waveguide laser [4-6]. The direct growth of lattice engineered rare-earth ion doped double tungstate thin layers on top of un-doped $KY(WO_4)_2$ substrates by liquid phase epitaxy (LPE) has led to many successful demonstrations [1, 2, 4-9]. However, the refractive index contrast between the grown layer and substrate is very low (<0.02), leading to large devices not compatible with on-chip integration. The quality of the high refractive index crystalline tungstate films grown on low-refractive index substrates (i.e., SiO_2) by pulsed laser deposition (PLD) is not yet good enough for device applications [10]. Recently, the heterogeneous transfer of un-doped $KY(WO_4)_2$ material onto a SiO_2 substrate led to the first demonstration of high refractive index contrast waveguides in $KY(WO_4)_2$ [11]. Such compact waveguides show great promise for the realization of on-chip lasers and amplifiers by hybrid integration with passive photonic platforms, such as silicon-on-insulator (SOI) and silicon nitride (Si_3N_4).

One of the biggest challenges to achieve passive-active integration is the optical coupling between photonic platforms within an integrated chip. In SOI platforms, vertical couplers have been used to couple the propagating field between the silicon waveguide and the integrated semiconductor gain medium [12-15]. By controlling the relative widths of the silicon and active gain material waveguide cores, the propagating mode location can be varied between the silicon and active core. In that way, a higher gain can be achieved than in devices in which the propagating field overlaps the active gain medium only by the evanescent field. The first practical demonstration of vertical couplers [16, 17] fabricated by flip-chip bonding between polymer and silicon chips has shown a promising way to enable large scale hybrid integration with low packaging and material cost. Compared to SOI platforms, the silicon nitride platform exhibits better performance in various aspects such as ultra-low propagation loss (0.1 dB/m at 1550 nm), and wide transmission window (~400 nm to 2350 nm) [18]. The hybrid integration [19-21] of rare-

*j.mu@utwente.nl; phone +31 53 489 2110; fax +31 53 489 3511; os.tnw.utwente.nl

Integrated Optics: Devices, Materials, and Technologies XX, edited by Jean-Emmanuel Broquin, Gualtiero Nunzi Conti, Proc. of SPIE Vol. 9750, 975012 · © 2016 SPIE
CCC code: 0277-786X/16/$18 · doi: 10.1117/12.2212206

earth ion doped active media onto Si_3N_4 chips supports the large spectral separation between pump and signal, which, in some cases, might fall outside the transparency window of SOI platforms.

This paper presents the design, fabrication, and characterization of adiabatic vertical couplers for the hybrid integration of silicon nitride single-stripe waveguide technology with polymer waveguides by flip-chip bonding. An efficient design flow to extract optimal parameters for the vertical couplers, obtain the adiabatic condition, and analyze the tolerance of the devices to fabrication errors is presented. The chosen optimal parameters are used to fabricate the couplers. In the fabrication, the process of SU-8 2000.5 is optimized in order to create polymer tapers with a nominal tip width of 0.8 μm. The flip-chip bonding process is also optimized to achieve a good alignment accuracy based on temporal contact tests. The polymer waveguides developed in this work are conceived as intermediate connectors between the silicon nitride passive waveguides and the active rare-earth ion doped $KY(WO_4)_2$ amplifiers. This integration will be presented in a later publication.

2. DEVICE DESIGN

2.1 Structure

Figure 1 shows a 3D schematic of the proposed vertical coupler, where a top polymer waveguide chip is flip-chip bonded onto the Si_3N_4 device. After bonding, the polymer waveguide fully contacts the Si_3N_4 waveguide core. The rest of the gap between the two chips is filled with an underfill adhesive, which serves as a cladding for both waveguide cores. The widths of both polymer and Si_3N_4 waveguide cores are tapered to improve coupling efficiency. During propagation, the confined mode in the input Si_3N_4 waveguide core [Fig. 1(a)] is firstly transferred to the combined core structure (CCS) at the taper tip of the polymer waveguide [Fig. 1(b)]. In the polymer taper region (i.e., between (b) and (c) in Fig. 1), the width of Si_3N_4 waveguide is kept constant. During the Si_3N_4 tapering, the width of the polymer waveguide is kept constant (i.e., between (c) and (d) in Fig. 1). By varying the relative width of polymer and Si_3N_4 waveguide cores, the supermode can be vertically transferred between the two waveguides. Negligible radiation losses can be obtained under adiabatic conditions in the tapered regions (i.e., between (b) and (d) in Fig. 1). Furthermore, the adiabatic couplers are reversible and present a broadband behavior as they are based on the mode transform principle.

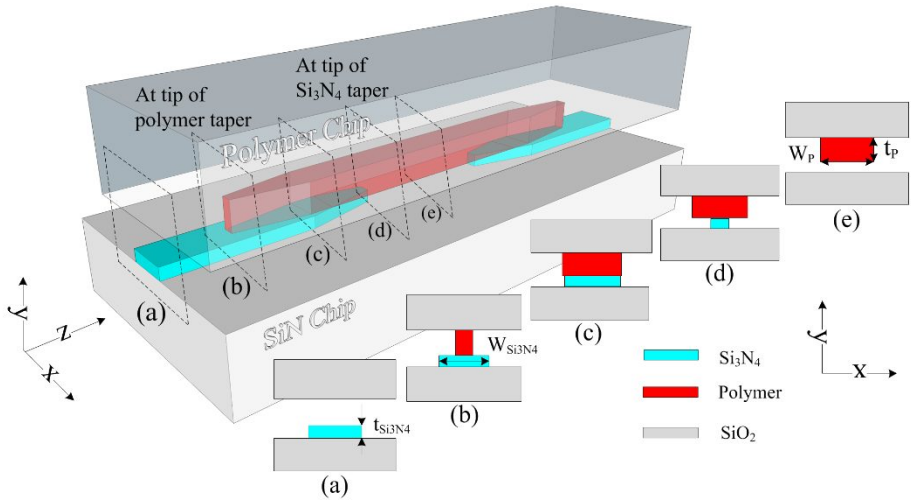

Figure 1. 3D schematic of the flip-chip bonded vertical coupler and its cross-sections at the Si_3N_4 input (a), the taper tip of polymer (b), the end/begin of polymer/Si_3N_4 taper (c), the taper tip of Si_3N_4 (d) and the polymer core (e). The figures are not to scale.

2.2 Design method

In the vertical coupler, two main origin of losses can be identified, one being at the start of the polymer waveguide taper [Fig. 1 (b)] and the other one at the end of the Si_3N_4 waveguide taper [Fig. 1 (d)]. At those points, sudden spatial perturbations are introduced by the taper tips. The loss due to the mismatch between the confined

fundamental mode in the Si_3N_4 core and the supermode in the CCS at the taper tip of the polymer waveguide is denoted by α_1. The loss due to the mode mismatch between the polymer core and the CCS at taper tip of the Si_3N_4 part is denoted by α_2. The mode mismatch losses can be neglected when the widths of the taper tips are so small that the mode cut-off condition is reached. In such case, the mode is fully transferred from the CCS to the other waveguide core without experiencing a perturbation at the tip. Such condition can be achieved when using electron-beam lithography (EBL) or stepper lithography, which can push the limit of the width of the SOI waveguide tapers to tens of nanometers [17, 22]. In this work, the size of the structures is limited by optical photolithography. The width of the tip of both the Si_3N_4 and polymer tapers is fixed to 0.8 μm. As the optical mode still exists for a core of such a width, the transmission loss of the vertical coupler, α_c, can be estimated by the sum of α_1 and α_2. In this theoretical analysis, other sources of propagation losses, such as absorption in the material, scattering due to the fabrication process, and reflections at the perturbations are neglected.

The cross-section of the Si_3N_4 and polymer cores need to be optimized to achieve high coupling efficiency and large tolerance to fabrication misalignments. The optimization process is based on the mode mismatch losses ($\alpha_{1,2}$), which can be calculated from mode overlap coefficients, $\Gamma_{1,2}$, at at corresponding cross-sections, $\alpha_{1,2} = -10 \cdot \log_{10} \Gamma_{1,2}$. The general expression of Γ is given by

$$\Gamma = \frac{|\iint E_a^*(x,y) E_b(x,y) dxdy|^2}{\iint |E_a^2(x,y)| dxdy \iint |E_b^2(x,y)| dxdy} \tag{1}$$

where E_a and E_b are the electric fields at the two cross-sections that meet at the tip of the polymer waveguide (i.e., cross sections (a) and (b) in Fig. 1) and at the tip of the Si_3N_4 waveguide (i.e., cross sections (d) and (e) in Fig. 1). A small width of the polymer core and a large width of the Si_3N_4 waveguide core at the taper tip of the polymer are desirable to reduce α_1, whereas the opposite is required at the Si_3N_4 taper tip. Studying the mode mismatches based on 2D cross-sections permits selecting the optimum widths of the two waveguide cores at the different locations along the vertical coupler. After that, the effect of the propagation angle in the tapered regions needs to be investigated by 3D simulations.

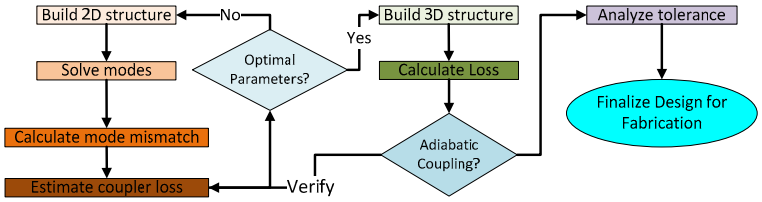

Figure 2. A design flow of adiabatic vertical coupler.

To obtain optimal design parameters with less consumption of time and computer memory, the design flow shown in Figure 2 is proposed in this work. In the first step, the optimal dimensional parameters of the 2D cross-sections as well as the refractive index of the underfill material are chosen from the results of mode mismatch calculations carried out with the film mode matching (FMM) method [23] using the commercial software OptoDesigner (PhoeniX B.V.). In the next step, 3D structures with the optimal parameters are built to simulate transmission losses using a 3D beam propagation method (3D-BPM) [24] from the commercial software OptoDesigner. A comparison between the transmission losses calculated by the 3D-BPM method and the ones estimated from mode mismatch calculations is performed to confirm the reliability of the optimal parameters. Such comparison is carried out for adiabatic angles in the taper regions. The last step is to analyze the tolerance to misalignment errors. The length of the tapers in this work has not been optimized. Such optimization of the taper structures could be realized by means of the use of multiple sections [25], and nonlinear tapers [26, 27]. However, it is out of scope of this study.

In this work, the negative epoxy-based photoresist SU-8, which is optically transparent at the telecommunication wavelengths [28, 29], is used to fabricate the core of the polymer waveguides. The ultraviolet light (UV) curable Norland Optical Adhesive (NOA-84) is used as the underfill adhesive during the flip-chip bonding process. The refractive indices of SU-8 and fully cured NOA-84 at the wavelength of 1550 nm, are 1.574 and 1.508 respectively as measured by Metricon prism coupling instrument. Three thicknesses of Si_3N_4 (t_{Tri}) including 70 nm, 90 nm, and 110 nm are studied. A range of SU-8 thickness (t_P), varying from 0.4 μm to 1.8 μm, is considered. Both the widths of Si_3N_4 (W_{Tri}) and SU-8 (W_P) waveguide cores are varied from 0.8 μm to 3.8 μm.

2.3 Simulation results

Figure 3(a) – 3(f) shows the losses due to mode mismatch for different dimensional parameters at 1550 nm wavelength. At the tip of the polymer taper (see cross-section (b) in Fig. 1), the thicker the Si_3N_4 core the lower the mode-mismatch loss, α_1, for a larger range of widths and thicknesses of the polymer waveguide. At the tip of the Si_3N_4 taper, a thinner Si_3N_4 core together with a larger polymer core in both width and thickness leads to a better mode field overlap and consequently a smaller α_2. The technology used in this work was restricted to layers of uniform thicknesses. With the values of these graphs, the optimal design parameters can be extracted.

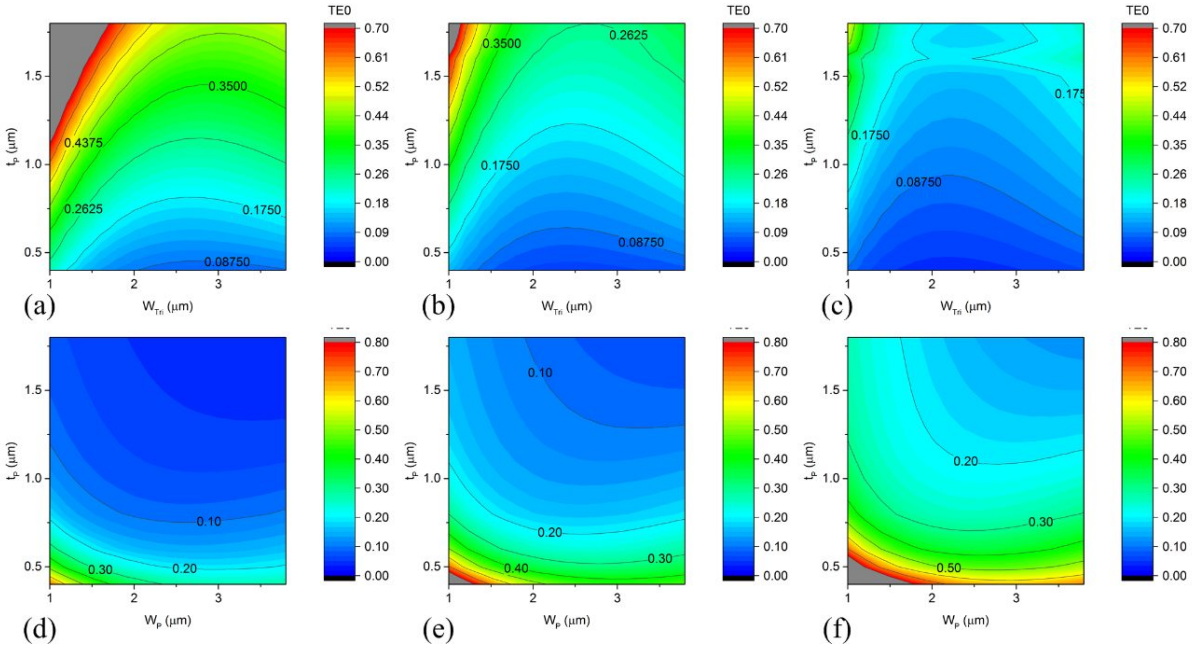

Figure 3. Calculated mode mismatch losses. α_1 at t_{tri} of 70 nm (a), 90 nm (b), and 110 nm (c). α_2 at t_P of 70 nm (d), 90 nm (e) and 110 nm (f). Both the widths of Si_3N_4 and polymer taper tips are 800 nm. Wavelength: 1550 nm.

For the experimental demonstration of this work, a polymer thickness of t_P of 0.5 µm was chosen. A polymer thickness of 0.5±0.1 µm can be reproducibly achieved by spin coating SU-8 2000.5 at a speed of 3000 rpm. $W_P = 3.5$ µm and $W_{Tri} = 3$ µm are then selected as widths for the polymer and the Si_3N_4 waveguide cores respectively for a 90 nm thick Si_3N_4 layer.

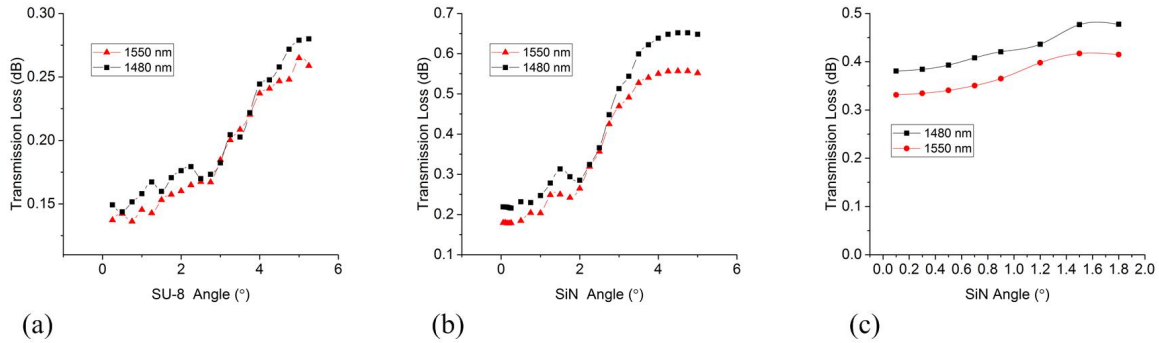

Figure 4.Transmission loss as a function of the angle of the taper angle for a flip-chip bonded 3D structure considering only the polymer taper (a), only the Si_3N_4 taper (b) and the whole vertical coupler (c) at the wavelength of 1480 nm and 1550 nm.

In order to obtain the adiabatic condition, the polymer and the Si_3N_4 tapers are studied separately. The 3D structure is built for the polymer taper starting from the Si_3N_4 input [Fig. 1(a)] to the cross-section where the polymer taper

ends [Figure 1(c)]. The transmission loss calculated by 3D-BPM of this section of the coupler taper as a function of polymer taper angle is shown in Figure 4(a). The 3D-BPM calculated transmission loss of the Si_3N_4 taper section [Fig. 1(c) to (e)] is shown in Figure 4(b). The angles below which the transmission losses become convergent are considered as the adiabatic angles. The Si_3N_4 taper is more sensitive to its angle variation than the polymer taper because of the higher sensitivity of mode size related to the change of the Si_3N_4 taper width. The convergence starts at 1° for the polymer taper and at 0.5° for the Si_3N_4 taper. The angle of the polymer taper was fixed at 0.25° while the angle of the Si_3N_4 taper was varied from 0.1° to 1.8°. The angle dependence of the transmission losses of the complete vertical coupler is shown in Figure 4(c). The transmission losses computed by the sum of α_1 and α_2 are 0.39 dB and 0.45 dB at the wavelength of 1550 nm and 1480 nm respectively. The losses calculated with 3D-BPM are ~0.06 dB smaller, showing a good agreement between the two simulation methods.

During the flip-chip bonding processes, the lateral misalignment, i.e., the shift in the x-direction, causes changes in the mode field distribution, therefore influencing the transmission losses. Figure 5 shows the transmission losses calculated by 3D-BPM simulations as a function of misalignment in the x-direction for both 1480 nm (a) and 1550 nm (b) wavelengths and different angles of the Si_3N_4 taper. The transmission losses calculated using 2D mode-overlap calculations are also included in Fig. 5. As the misalignment increases, an oscillation phenomenon is observed in the 3D-BPM simulations. Although not completely understood yet, it is believed that such oscillation is due to mode coupling effects between the polymer and Si_3N_4 waveguide cores. Smaller taper angles leads to longer tapers. The longer interaction length leads to more oscillations as it can be seen in Figure 5. Other factors that could introduce errors in these simulations, such as the grid size utilized, are currently being studied. In order to obtain transmission losses of less than 1 dB, the lateral shift has to be limited within ±0.5 μm. In the simulations, the effect of tilt in the X-Y direction was neglected as well as the misalignment in the z-direction.

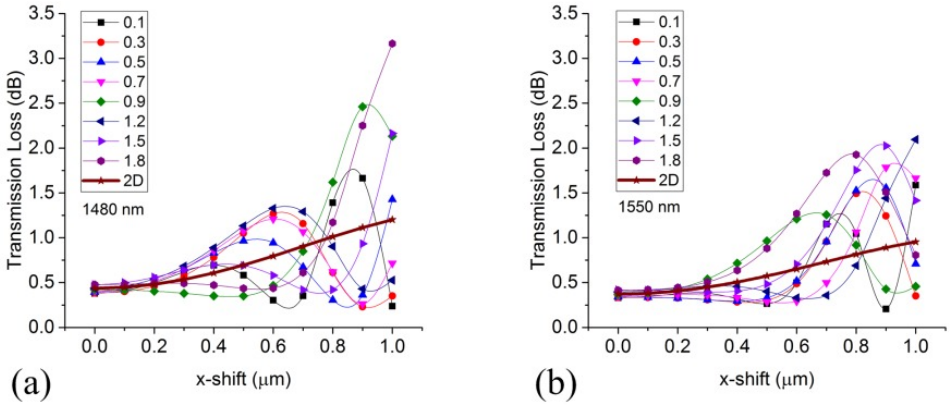

Figure 5. Transmission of vertical couplers as a function of lateral misalignments for a range of Si_3N_4 taper angles varying from 0.1° to 1.8°. The wavelengths of 1480 nm (a) and 1550 nm (b) are considered.

3. FABRICATION OF VERTICAL COUPLER

The Si_3N_4 chip and polymer chip are fabricated separately. A thermally oxidized silicon wafer with 15 μm thick SiO_2 layer is employed as the substrate for the Si_3N_4 chip. The substrate for the polymer chip is borosilicate glass so that the structures can be visible after bonding for checking the alignment accuracy. Both Si_3N_4 chip and polymer chip have the same dimensions (12 mm × 5 mm).

3.1 Si_3N_4 chip

The Si_3N_4 devices were fabricated by LioniX B.V. Firstly, a Si_3N_4 layer is deposited using low-pressure chemical vapor deposition (LPCVD). The thickness of the deposited layer is measured to be 92.1 ± 0.6 nm by ellipsometer (Woollam M-20000UI). In the next step, the waveguide structures are patterned by optical lithography followed by reactive ion etching (RIE) and resist removal. During dry etching, a rate monitor is used to control the etching depth. The measured step height from the top of the Si_3N_4 core to the SiO_2 undercladding is 182 nm, as characterized by a Dektak profilometer, indicating a ~90 nm etched depth into the SiO_2. Figure 6(a) – 6(f) shows the profile of a Si_3N_4 taper at different locations along the taper tip using an atomic force microscope (AFM Bruker FastScan). The waveguide profiles are as expected except at the taper tips (nominal width ~0.8 μm). Such deformation of the taper

tip could be caused by a defect of the patterned photoresist during lithography. The roughness of the top area of the straight waveguide core and of the taper tip are measured to be less than 1 nm and 10 nm (Rms) respectively.

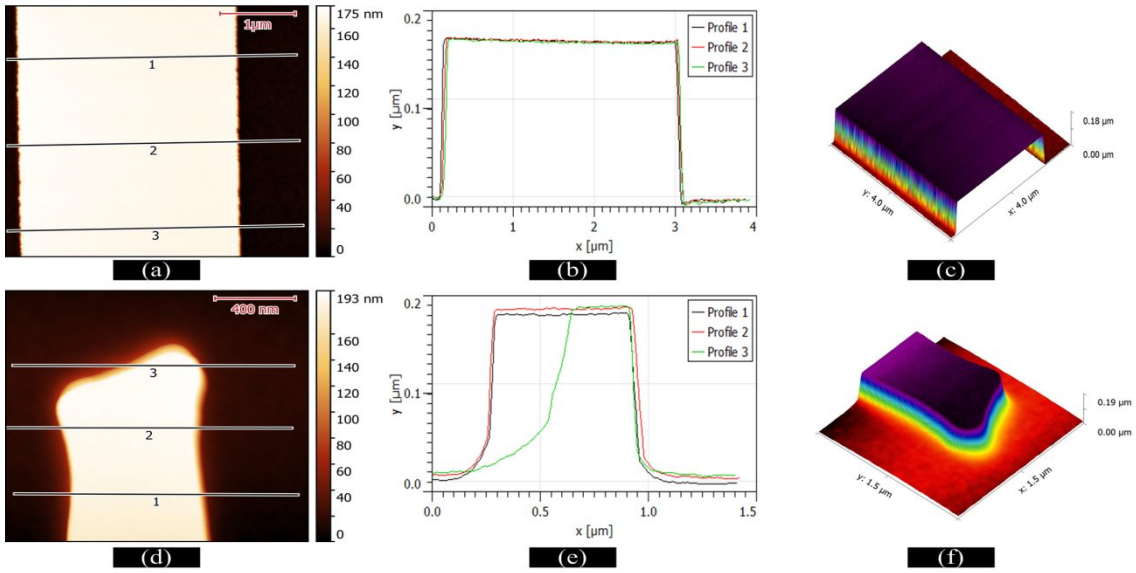

Figure 6. The AFM scanned results of Si_3N_4 waveguide at nominal width of 3 μm (a)-(c) and at the taper tip (d)-(f). The corresponding height profiles at different locations (b) and (e), and 3D profiles (c) and (f).

3.2 Polymer chip

The process of SU-8 waveguides consists of spin coating, soft bake, UV lithography, post-exposure bake and development. The deposited SU-8 2000.5 film is soft baked at 95 °C for 3 minutes to remove the solvent inside. After cooling down to room temperature (20 °C), the film is exposed to UV light (12 mW/cm^2) with a 365 nm filter and waveguides are patterned from photolithographic mask. Vacuum contact mode is used to minimize the near field (Fresnel) diffraction caused by the gap between the film and the mask. Then, the sample follows a post-exposure bake (PEB) to accelerate cationic polymerization initiated through exposure. After PEB step, the sample is developed after gradually being cooled down to room temperature on hotplate.

The exposure time and PEB are modified during the process because they affect cross-linking of epoxy. Two main problems were observed during the process development. The first one is that the thickness of the SU-8 waveguide gradually reduces at the taper tip region when the width decreases. The second one is the detachment of the waveguides from the substrate during the development step. The reduction of thickness and the detachment issues can be caused by insufficient polymerization and excessive stress. Better resolution of the waveguide profile can be achieved by fast polymerization when the photo-acid diffusion into non-exposed areas is weak [30]. However, it can cause big residual stress in the SU-8 film, leading to the detachment of the SU-8 waveguides, especially at the taper tips. The stress is a combination of intrinsic and extrinsic stresses [28]. The former is mainly generated during cross-linking during the PEB process, and the latter is mainly due to the thermal stress between the waveguide and the substrate and other externally applied forces.

The issues can be overcome either by absorbing higher dose of UV light or by following a slower PEB step. However, too long exposure time results in an increase of the width of channels. An optimization of the exposure time and PEB was performed. Finally, multiple temperature steps during the PEB step of the SU-8 2000.5 were used, including baking at 50 °C for 1 min, 65 °C for 3 min and 80 °C for 3 min with a temperature ramping speed of 2 °C/min. Exposure time above 45 s is necessary when using a 365 nm filter. The resulting width increase is ranges from 0.1 μm to 0.5 μm for different waveguides at an exposure time of 45 s. Figure 7(a) – 7(f) shows the AFM results of the fabricated SU-8 taper tip. The width of flat top of SU-8 waveguide core is found to be 3.4 ± 0.1 μm (i.e., nominal width 3.5 μm) while the bottom is about 3.8 ± 0.1 μm. The thickness of the taper only decreases at the roundly etched taper tip. Additionally, the rms roughness at the top of taper tip (~20 nm) is not as good as the one of straight waveguide core (~4 nm).

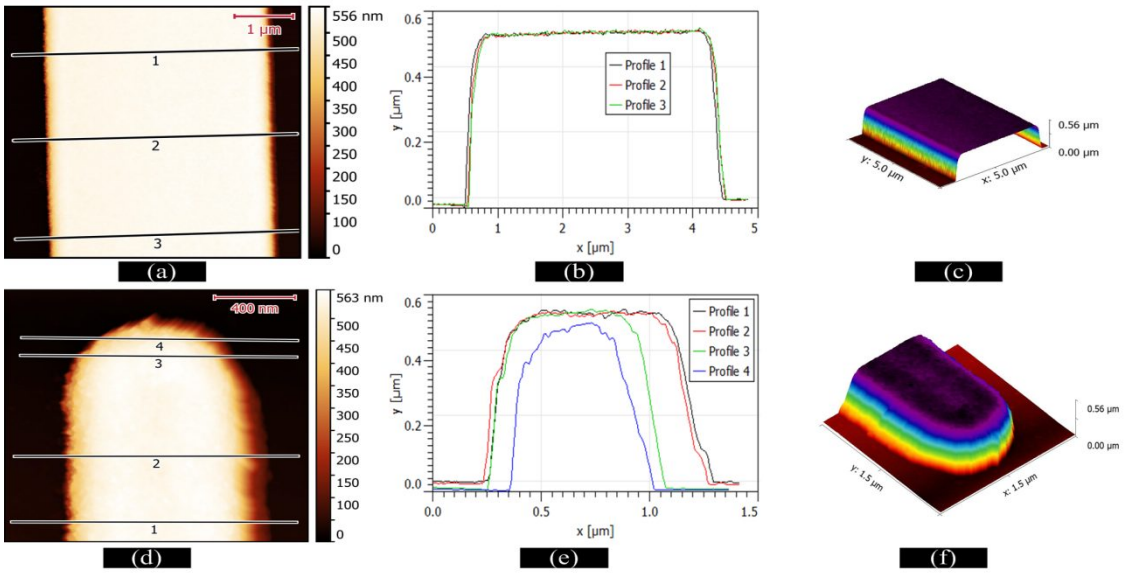

Figure 7. The AFM scanned results of SU-8 waveguide at nominal width of 3 µm (a) and at the taper tip (d). The corresponding profiles at different locations (b) and (e), and 3D profiles (c) and (f).

3.3 Flip-chip bonding assembly

The polymer chip is flip-chip bonded onto the Si_3N_4 chip by using a high precision flip-chip bonder (Finetech Lambda Fineplacer) with a nominal alignment accuracy of ~0.5 µm. The waveguides in the polymer chip and Si_3N_4 chip are aligned visually. In order to optimize the placement accuracy prior to permanent bonding, the two chips are temporarily bonded by implementing a minimum force of 4N and heating up the bottom stage to 60 °C, which allows the user to check the accuracy of the bonding at different positions on the chip. After a sufficient alignment accuracy has been achieved, the polymer chip is picked up. A suitable volume of NOA-84 glue is then dropped on the top of the Si_3N_4 chip. In order to achieve a full contact between the surface of the polymer and the Si_3N_4 cores but without deforming the polymer waveguides, the bonding force is set to 10 N with a ramping speed of 1 N/s. The stage is set to 60 °C so that the viscosity of the underfill adhesive is lower than at room temperature. The flip-chip bonding process is shown in Figure 8(a). The Vernier rulers (0.25 µm resolution) on both the left and right sides of the chip are separated by a distance of 0.9 mm. Lateral misalignments of –0.75 µm and +1.25 µm can be visually found from the Vernier rulers, where "+"and "–" mean the polymer chip shifts in either positive or negative x-direction. Furthermore, the couplers at different locations inside the chip have different misalignments, which can be specifically calculated from the mask layout.

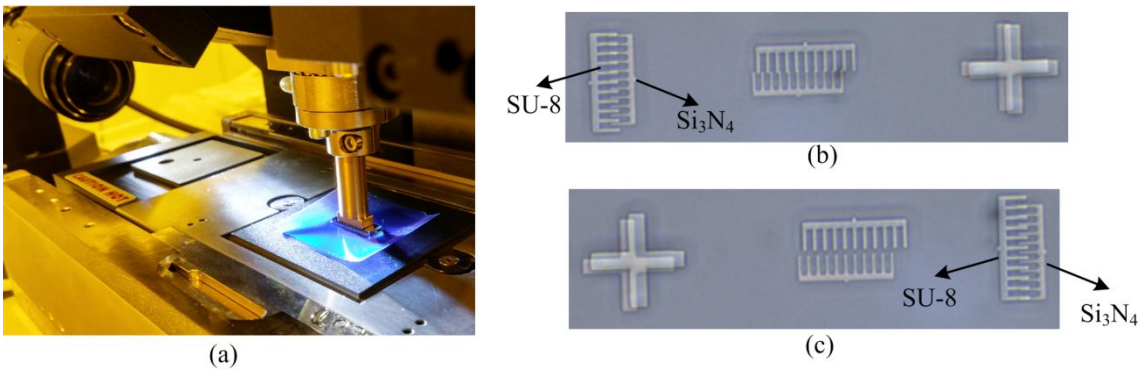

Figure 8. (a) Chip bonding by using flip-chip bonder. Vernier rulers on (b) left side and right (c) side of the bonded chip separated by a distance of 0.9 mm.

4. CHARACTERIZATION RESULTS

The vertical couplers are characterized at the wavelengths of 1480 nm and 1550 nm. A tunable laser (Agilent 8164B) is employed. A single mode polarization maintaining fiber (PM980-XP) is used to couple into the chip and an ordinary single mode fiber is employed to collect the field at the output. The mode field diameters (MFD) of both fibers are ~10 ± 0.5 μm. The input power at 1480 nm is -5.2 dBm, and the one at 1550 nm is -4.9 dBm. The alignment of the input coupling is done at 1550 nm. After optimization, the position of the input stage is fixed for the measurements at both wavelengths. The measured transmissions (dBm) at the wavelength of 1480 nm and 1550 nm are shown in Figure 9(a) and 9(b) respectively.

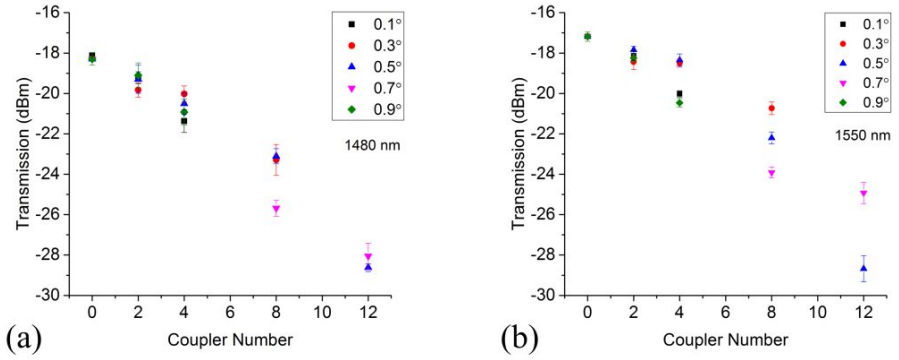

Figure 9. The measured transmission (dBm) of waveguides at the wavelengths of (a) 1480 nm and (b) 1550 nm for different angles of the Si_3N_4 tapers. Each waveguide has a different number of cascaded couplers. "0" represents the reference Si_3N_4 waveguide.

An index matching fluid is used to improve fiber to chip butt-coupling. The computed coupling loss due the mode mismatch between the fiber mode (MFD: 10 μm) and the mode of the input/output Si_3N_4 waveguide (i.e., width of 3 μm) was calculated as 6.6 dB at 1480 nm and 6.1 dB at 1550 nm. Therefore, the expected transmission of the reference waveguide are -18.4 dBm and -17.1 dBm at 1480 nm and 1550 nm respectively. The values closely match the measured transmission of the reference waveguide, which are -18.1 dBm and -17.2 dBm at 1480 nm and 1550 nm respectively. Assuming that the coupling losses of all input facets are similar, it is reliable to obtain the losses of all devices by subtracting the transmission of the reference waveguide. The loss of the different devices consisting of waveguide with couplers mainly originates from the total loss of the cascaded couplers. However, extraction of the loss of a coupler with specific misalignment is difficult because couplers at different locations have different misalignments.

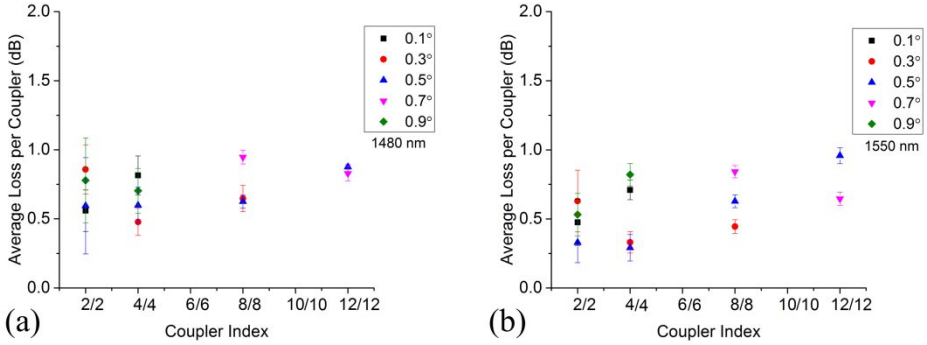

Figure 10. The average loss of coupler for different angles of Si_3N_4 tapers at the wavelengths of (a) 1480 nm and (b) 1550 nm.

Therefore, in order to obtain an estimate value, the total losses of a device are simply divided by the number of couplers on that waveguide. Figure 10(a) and 10(b) show the average loss per coupler calculated in the described way. The values of the average loss per coupler are found to below 1 dB for the fabricated couplers at both 1480 nm

and 1550 nm wavelengths. The dispersion of the data could be due to variation in the input coupling conditions between different devices.

5. CONCLUSION

In this paper, flip-chip bonded adiabatic vertical couplers between polymer chips and silicon nitride chips for hybrid integration applications are design, fabricated and experimentally characterized. The couplers are designed using a combination of 2D FMM mode solver and 3D BPM simulations, requiring less consumption of time and computer memory. The method enables users to extract optimal parameters through an amount of calculations of mode mismatch losses, and then focus on studying the adiabatic conditions and analyzing the tolerance of the optimal design using 3D simulations. Under adiabatic operation, the designed adiabatic couplers show transmission losses below 0.5 dB at both the wavelengths of 1550 nm and 1480 nm. The optimizations of SU-8 2000.5 process and flip-chip bonding process were introduced. The fabricated chip exhibit average loss per coupler below 1 dB for vertical couplers with different angles of Si_3N_4 tapers.

ACKNOWLEDGEMENT

The authors would like to acknowledge financial support from the "Stichting voor de Technisch Wetenschappen" (STW) under the project numbers STW-12832 and STW-13536. J. Mu acknowledges financial support from China Scholarship Council. M. Hoekman, K. Wörhoff, R. Stoffer and A. Leinse are thanked for useful discussions.

REFERENCES

[1] D. Geskus, S. Aravazhi, K. Wörhoff *et al.*, "High-power, broadly tunable, and low-quantum-defect $KGd_{1-x}Lu_x(WO_4)_2:Yb^{3+}$ channel waveguide lasers," Optics Express, 18(25), 26107-26112 (2010).

[2] D. Geskus, S. Aravazhi, S. M. Garcia-Blanco *et al.*, "Giant Optical Gain in a Rare-Earth-Ion-Doped Microstructure," Advanced Materials, 24(10), OP19-OP22 (2012).

[3] H. Jianhong, L. Jipeng, S. Rongbing *et al.*, "Short pulse eye-safe laser with a stimulated Raman scattering self-conversion based on a Nd:KGW crystal," Optics Letters, 32(9), 1096-1098 (2007).

[4] K. van Dalfsen, S. Aravazhi, C. Grivas *et al.*, "Thulium channel waveguide laser with 1.6 W of output power and ~80% slope efficiency," Optics Letters, 39(15), 4380-4383 (2014).

[5] K. van Dalfsen, S. Aravazhi, C. Grivas *et al.*, "Thulium channel waveguide laser in a monoclinic double tungstate with 70% slope efficiency," Optics Letters, 37(5), 887-889 (2012).

[6] K. van Dalfsen, S. Aravazhi, D. Geskus *et al.*, "Efficient $KY_{1-x-y}Gd_xLu_y(WO_4)_2:Tm^{3+}$ channel waveguide lasers," Optics Express, 19(6), 5277-5282 (2011).

[7] J. W. Kim, S. Y. Choi, D.-I. Yeom *et al.*, "Yb:KYW planar waveguide laser Q-switched by evanescent-field interaction with carbon nanotubes," Optics Letters, 38(23), 5090-5093 (2013).

[8] D. Geskus, S. Aravazhi, C. Grivas *et al.*, "Microstructured $KY(WO_4)_2:Gd^{3+}$, Lu^{3+}, Yb^{3+} channel waveguide laser," Optics Express, 18(9), 8853-8858 (2010).

[9] D. Geskus, S. Aravazhi, E. Bernhardi *et al.*, "Low-threshold, highly efficient Gd^{3+}, Lu^{3}+ co-doped $KY(WO_4)_2:Yb^{3+}$ planar waveguide lasers," Laser Physics Letters, 6(11), 800-805 (2009).

[10] M. Jelinek, J. Lančok, M. Pavelka *et al.*, "Optical and waveguiding properties of Nd:KGW films grown by pulsed laser deposition," Applied Physics A, 74(4), 481-485 (2002).

[11] M. A. Sefunc, V. Vaiti, M. Dijkstra *et al.*, "Towards on-chip high index contrast rare-earth-doped potassium double tungstate amplifiers," Proc. ICTON, 1-4 (2015).

[12] L. Lever, Z. Ikoni, and R. W. Kelsall, "Adiabatic mode coupling between SiGe photonic devices and SOI waveguides," Optics Express, 20(28), 29500-29506 (2012).

[13] B. Ben Bakir, A. Descos, N. Olivier *et al.*, "Electrically driven hybrid Si/III-V Fabry-Pérot lasers based on adiabatic mode transformers," Optics Express, 19(11), 10317-10325 (2011).

[14] S. Keyvaninia, G. Roelkens, D. Van Thourhout *et al.*, "Demonstration of a heterogeneously integrated III-V/SOI single wavelength tunable laser," Optics Express, 21(3), 3784-3792 (2013).

[15] M. Lamponi, S. Keyvaninia, F. Pommereau *et al.*, "Heterogeneously integrated InP/SOI laser using double tapered single-mode waveguides through adhesive die to wafer bonding," Proc. Group IV Photonics (GFP), 22-24 (2010).

[16] R. Dangel, J. Hofrichter, F. Horst *et al.*, "Polymer waveguides for electro-optical integration in data centers and high-performance computers," Optics Express, 23(4), 4736-4750 (2015).

[17] I. M. Soganci, A. La Porta, and B. J. Offrein, "Flip-chip optical couplers with scalable I/O count for silicon photonics," Optics Express, 21(13), 16075-16085 (2013).
[18] K. Wörhoff, R. G. Heideman, A. Leinse *et al.*, "TriPleX: a versatile dielectric photonic platform," Advanced Optical Technologies, 4(2), 189-207 (2015).
[19] W. Lei, G. Ruimin, W. Bing *et al.*, "Hybrid Si_3N_4-Er/Yb Silicate Waveguides for Amplifier Application," Photonics Technology Letters IEEE, 24(11), 900-902 (2012).
[20] M. Belt, and D. J. Blumenthal, "Erbium-doped waveguide DBR and DFB laser arrays integrated within an ultra-low-loss Si_3N_4 platform," Optics Express, 22(9), 10655-10660 (2014).
[21] M. Piels, J. F. Bauters, M. L. Davenport *et al.*, "Low-Loss Silicon Nitride AWG Demultiplexer Heterogeneously Integrated With Hybrid III-V/Silicon Photodetectors," Journal of Lightwave Technology, 32(4), 817-823 (2014).
[22] J. Shu, C. Qiu, X. Zhang *et al.*, "Efficient coupler between chip-level and board-level optical waveguides," Optics Letters, 36(18), 3614-3616 (2011).
[23] A. S. Sudbo, "Film mode matching: a versatile numerical method for vector mode field calculations in dielectric waveguides," Pure and Applied Optics: Journal of the European Optical Society Part A, 2(3), 211 (1993).
[24] W. P. Huang, and C. L. Xu, "Simulation of three-dimensional optical waveguides by a full-vector beam propagation method," Quantum Electronics, IEEE Journal of, 29(10), 2639-2649 (1993).
[25] J. Zou, Y. Yu, M. Ye *et al.*, "Short and efficient mode-size converter designed by segmented-stepwise method," Optics Letters, 39(21), 6273-6276 (2014).
[26] M. Jinfeng, M. A. Sefunc, and S. M. Garcia-Blanco, "Design and length optimization of an adiabatic coupler for on-chip vertical integration of rare-earth-doped double tungstate waveguide amplifiers," Proc. ICTON, 1-4 (2014).
[27] Y. Fu, T. Ye, W. Tang *et al.*, "Efficient adiabatic silicon-on-insulator waveguide taper," Photonics Research, 2(3), A41-A44 (2014).
[28] K. Stephan, B. Gabriela, L. Michael *et al.*, "Processing of thin SU-8 films," Journal of Micromechanics and Microengineering, 18(12), 125020 (2008).
[29] J. M. Ruano-López, M. Aguirregabiria, M. Tijero *et al.*, "A new SU-8 process to integrate buried waveguides and sealed microchannels for a Lab-on-a-Chip," Sensors and Actuators B: Chemical, 114(1), 542-551 (2006).
[30] G. P. Patsis, E. Gogolides, and K. V. Werden, "Effects of Photoresist Polymer Molecular Weight and Acid-Diffusion on Line-Edge Roughness," Japanese Journal of Applied Physics, 44(8R), 6341 (2005).